The Changes in Ca^{2+} Sparks Associated with Measured Modifications of Intra-store Ca^{2+} Concentration in Skeletal Muscle

Bradley S. Launikonis,[1] Jingsong Zhou,[1] Demetrio Santiago,[1] Gustavo Brum,[2] and Eduardo Ríos[1]

[1]Section of Cellular Signaling, Department of Molecular Biophysics and Physiology, Rush University, Chicago, IL 60612
[2]Departamento de Biofísica, Universidad de la República, Facultad de Medicina, Montevideo, Uruguay

In cardiac muscle and amphibian skeletal muscle, the intracellular Ca^{2+} release that signals contractile activation proceeds by discrete local packets, which result in Ca^{2+} sparks. The remarkably stereotyped duration of these release events requires a robustly timed termination mechanism. In cardiac muscle the mechanism of spark termination appears to crucially involve depletion of Ca^{2+} in the lumen of the sarcoplasmic reticulum (SR), but in skeletal muscle, the mechanism is unknown. We used SEER (shifted excitation and emission ratioing of fluorescence) of SR-trapped mag-indo-1 and confocal imaging of fluorescence of cytosolic rhod-2 to image Ca^{2+} sparks while reversibly changing and measuring $[Ca^{2+}]$ in the SR ($[Ca^{2+}]_{SR}$) of membrane-permeabilized frog skeletal muscle cells. Sparks were collected in cells immersed in a solution promoting production of events at moderate frequency. Just after permeabilization, event frequency was zero, and in 10 minutes it reached close to a steady value. Controlled interventions modified $[Ca^{2+}]_{SR}$ reversibly between a low value (299 μM on average in 10 experiments) and a high value (433 μM, a 45% average increase). This change increased sparks frequency by 93%, spatial width by 7%, rise time by 10%, and peak amplitude by 38% (provided that it was calculated in absolute terms, rather than normalized by resting fluorescence). The changes in event frequency and amplitude were statistically significant. The "strength" of the effect of $[Ca^{2+}]_{SR}$ on frequency, quantified by decomposition of variance, was <6%. While the average change in $[Ca^{2+}]_{SR}$ was limited, it reached up to 200% in individual fibers, without causing massive Ca^{2+} release or an increase of >3.5-fold in event frequency. Taken together with existing evidence that depletion is modest during Ca^{2+} sparks or release elicited by an action potential, the mild effects of $[Ca^{2+}]_{SR}$ reported here do not support a major role of depletion in either the termination of sparks or the strong inactivation that terminates Ca^{2+} release at the global level in frog skeletal muscle.

The Journal of General Physiology

INTRODUCTION

The rapid Ca^{2+} signal that controls the contraction of fast twitch skeletal muscle must first increase cytosolic $[Ca^{2+}]$ ($[Ca^{2+}]_{cyto}$) sufficiently rapidly to saturate the contractile filament protein troponin C, and then restore essentially Ca^{2+}-free conditions, all in as little as 3 ms in some muscles (Rome, 2006). To achieve these rapid Ca^{2+} transients, multiple mechanisms ensure that a large fraction of the Ca^{2+} release channels of the sarcoplasmic reticulum (SR) open in less than a millisecond, while other mechanisms ensure their equally rapid closure. A feature of the intracellular release channels (ryanodine receptors [RyRs]) that is central to their control is their ability to be gated by the permeant ion. This mechanism of opening has been called Ca^{2+}-induced Ca^{2+} release, or CICR (Endo et al., 1970). CICR is mediated by a cytosol-facing site on the channel, at which Ca^{2+} binding, with half saturation in the low μM, opens the channel.

Solid evidence for a second activating mechanism, involving a site or "sensor" facing the SR lumen, has emerged in the heart (for review see Györke et al., 2002). This site may be located on the protein calsequestrin (CSQ; Györke et al., 2004). The increase in frequency of local Ca^{2+} release events (Ca^{2+} sparks) and cardiac cell- and tissue-wide Ca^{2+} waves observed upon Ca^{2+} store overload (Shannon et al., 2000) are attributed to activation of this controlling site.

The evidence for an intra-store activating site in skeletal muscle is less conclusive. Tripathy and Meissner (1996) emphasized the difficulty of separating direct effects from indirect cytosolic actions of lumenal Ca^{2+} in bilayer studies. Others suggest that CSQ may function as a lumenal calcium sensor (Beard et al., 2005), although the physiological importance of this role has not been established. Cellular studies show dual effects. In experiments that derived SR Ca^{2+} content from integral measures of Ca^{2+} release it was concluded that substantial depletion of the store determines an increase in the Ca^{2+} release permeability elicited by membrane depolarization (Pape and Carrier, 1998; Pape et al., 1998;

Correspondence to Eduardo Rios: erios@rush.edu

Abbreviations used in this paper: CICR, Ca^{2+}-induced Ca^{2+} release; FWHM, full width at half magnitude; RyR, ryanodine receptor; SEER, shifted excitation and emission ratioing of fluorescence; SR, sarcoplasmic reticulum.

Pizarro and Ríos, 2004). The results are consistent with the observation of a constant amount of Ca^{2+} released by an action potential at different total SR content in rat EDL and toad iliofibularis (Posterino and Lamb, 2003). This effect is opposite to the load-induced release observed in cardiac muscle.

On the other hand, there are reports of a load-induced increase of release in skeletal muscle. Lamb et al. (2001) showed that sensitivity to caffeine is strongly dependent on SR load in rat EDL. Zhou et al. (2004) found that the photolytic uncaging of Ca^{2+} in the cytosol of both amphibian and mammalian muscle was followed after a variable lag by an increase in spark frequency and occasionally massive release. They attributed the greater release to a dependence of channel activity on SR load that presumably also explains the enhanced sensitivity to caffeine. However, no potentiation of voltage-induced release by load was found, consistent with the conclusion that caffeine and depolarization favor channel opening through different pathways (Lamb et al., 2001). In this view, caffeine facilitates CICR, a mechanism intrinsically sensitive to load and manifested through sparks at the local level, while depolarization-operated release exhibits the opposite relationship with SR load.

In this study we used SEER (shifted excitation and emission ratioing of fluorescence; Launikonis et al., 2005) to image simultaneously intra-SR and cytosolic $[Ca^{2+}]$ in amphibian muscle. Thus we could collect sparks and compare their frequency and properties at various, measured $[Ca^{2+}]_{SR}$. Knowing the steady relationship between $[Ca^{2+}]_{SR}$ and spark activity, we were able to make inferences regarding putative roles of Ca^{2+} depletion in the control of Ca^{2+} release, and more specifically in the termination of Ca^{2+} sparks.

MATERIALS AND METHODS

Imaging was performed on single semitendinosus muscle fibers of *Rana pipiens*. Frogs were killed by decapitation under anesthesia, a procedure approved by the IACUC of Rush University. Muscles were incubated for 120 min at 18°C in Ringer solution with 10 μM mag-indo-1 AM. Fiber segments were mounted stretched under pins and membrane permeabilized with 0.002% saponin as previously described (Launikonis et al., 2005). Experiments were performed at 20–22°C.

Solutions

Ringer solution contained (in mM) NaCl (115), KCl (2.5), $CaCl_2$ (2.5), and tris-maleate (10), with pH adjusted to 7.4 with NaOH. A 0 Ca, 0 ATP, "relaxing" solution was used (with the addition of saponin) for permeabilizing the surface membrane and was also used to decrease $[Ca^{2+}]_{SR}$ via leak through the SR Ca^{2+} pump (Launikonis et al., 2005); it contained (in mM) K Glutamate (120), EGTA (1), $MgCl_2$ (2), NaCl (5), tris maleate (5), and 4% dextran, with pH adjusted to 7.1 with KOH. The reference internal solution contained K Glutamate (70.6), Na_2ATP (5), Na_2 creatine phosphate (10.29), EGTA (1), glucose (5), HEPES (10), dextran (8%), BTS (*n*-benzyl-*p*-toluene sulphonamide, 50 μM; Sigma-Aldrich), rhod-2 (100 μM), $CaCl_2$ (0.186), and $MgCl_2$ (4.96) for nominal $[Ca^{2+}]$ of 100 nM and $[Mg^{2+}]$ of 0.4 mM. $[CaCl_2]$ was varied to achieve $[Ca^{2+}]$ of 100, 400, or 800 nM. pH was adjusted to 7.1. The osmolality of all solutions was 260 ± 10 mosmol kg^{-1}.

Microscopy and Image Processing

SEER imaging was performed as previously described (Launikonis et al., 2005) using an AOBS confocal system (TCS SP2; Leica Microsystems). Line scan (*x-t*) images were acquired at 1.25 ms/line and 0.138 μm/pixel. *x-y* scans were acquired at the same rate and 0.23 μm/pixel. Monitoring of $[Ca^{2+}]$SR required two interleaved images, $F_1(x, y)$ and $F_2(x, y)$ of mag-indo-1 trapped in organelles (largely SR), while $[Ca^{2+}]$cyto was monitored by $F_3(x, y)$ or $F_3(x, t)$ of fluorescence of cytosolic rhod-2, with excitation lines and emission bands described by Launikonis et al. (2005). SEER ratio images $R(x, y) = F_1(x, y)/F_2(x, y)$ were used to derive $[Ca^{2+}]$ according to Eq. 1 in Launikonis et al. (2005).

Improved Detection of Sparks

In either *x-t* or *x-y* scans, sparks were identified automatically by a detection program. The detector, evolved from earlier versions (Cheng et al., 1999; González et al., 2000), was improved to deal with a wide range of event frequencies and to carry out the automatic calculation of "absolute spark amplitude," defined as increase in fluorescence, ΔF, rather than the usual $\Delta F/F_0$. (For simplicity, we write F instead of F_3 in this section.)

The work of the detector is illustrated in Fig. 1. Panel A shows a raw *x-t* image. A first analysis removed areas of this image above a low threshold ("sparky" areas) to obtain the "resting" image $F_0(x, t)$, which is not defined in sparky areas. The average of F_0 over x was a function $F_0(t)$ that decayed slowly and exponentially as a result of bleaching. An image corrected for bleaching, $F_B(x, t)$, was then generated, dividing $F(x, t)$ by a normalized $F_0(t)$ (i.e., $F_0(t)/\text{mean}(F_0(t))$). A resting fluorescence $F_0(x)$ was obtained, eliminating the sparky areas from $F_B(x, t)$ and averaging the result over t. Finally $F/F_0(x, t)$, a normalized image corrected for bleaching, was generated as the ratio of $F_B(x, t)$ and $F_0(x)$.

The detection of events was performed on a band-pass filtered version of $F/F_0(x, t)$. Improved detection was achieved by addition of criteria of exclusion to the detector. As in our original version (Cheng et al. 1999), the detector started by (1) locating all areas of the corrected image that were above a low intensity threshold (T_l), and then validating these areas individually by eliminating all those that (2) did not rise above a high threshold (T_h). The new version added five other criteria, excluding detected areas that (3) were <3.75 ms in duration, (4) were <0.4 μm in (maximum) width, (5) had an area of <15 pixels, (6) had a "signal," i.e., the integral of $F/F_0 - 1$ over its area that did not reach a minimum (T_s), or (7) had a signal density, ratio of signal over area, that did not reach a minimum (T_{ds}). The values of the seven criteria defined above were set empirically through extensive trial and error, seeking to minimize the number of undetected events that the eye judged to be valid, and the number of detections that appeared to be invalid. While this setting of criteria was dependent on the judgment of one observer, and of course not unique or even optimal, the values chosen were then used consistently, for every image of every experiment. Fig. 1 C shows the regions above T_l in the events that passed validation. The program completes its task by determining the "morphometric" spark parameters on each of these events. Parameters include amplitude (maximum of $F/F_0 - 1$), full width at half magnitude (FWHM, the spatial extent at the time of the peak where F/F_0 was greater than 1 + 0.5 × amplitude) and rise time (time lapse of rise between 10% and peak, measured on a three-pixel central average of F/F_0).

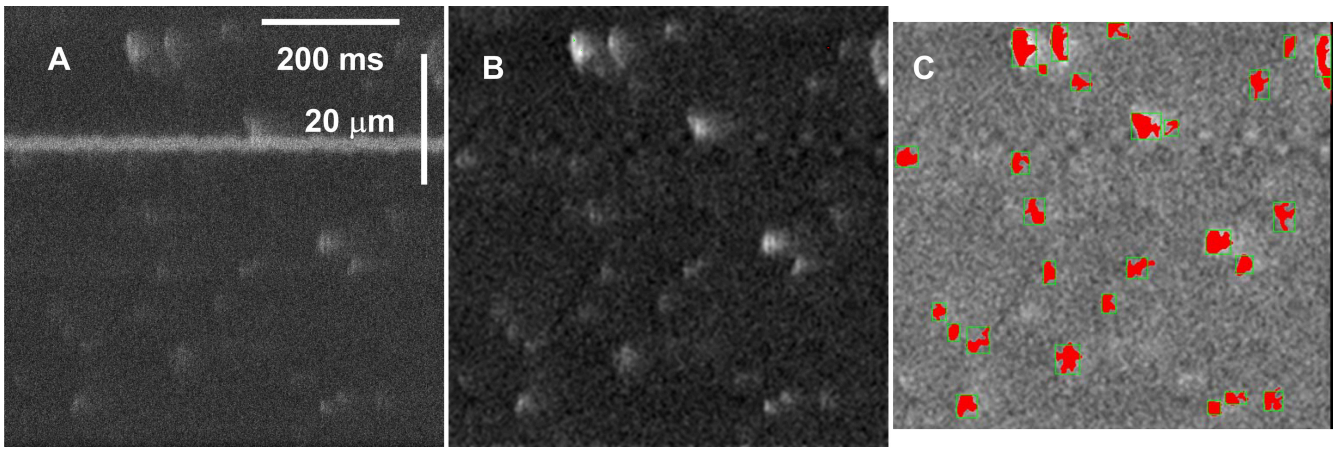

Figure 1. Performance of the automatic detector. The panels illustrate three stages of detection: A, the raw image, with several features that may cause detection problems, including high frequency of relatively small events, one large steady inhomogeneity, and noise; B, the bleaching-corrected, normalized, band pass–filtered image, which is subjected to the detection algorithm; C, normalized image, with red areas marking the suprathreshold "footprints" of events that passed all validation criteria described in the text. Spatial "margins" where filtering is imperfect due to edge effects are omitted in the final detection analysis. Identifier 061004a, image 125 ($[Ca^{2+}]_{SR}$ was 0.7 mM).

An Additional Spark Parameter, Absolute Amplitude

Unexpected features of the conventional spark amplitude, which is determined on F/F_0, led us to define and determine a spark amplitude in absolute terms, that is, without normalization, to avoid uncontrolled variations of F_0. Absolute amplitude is defined as the peak value of ΔF (or $F - F_0$). Fluorescence intensity is approximately proportional to the local concentration of Ca^{2+}-bound dye, which in these experiments is a measure of $[Ca^{2+}]$ because dye concentration was kept constant. The proportionality constant depends on five scanner parameters: exciting light intensity, photomultiplier voltage, scanning rate, pixel distance (or "zoom"), and confocal aperture diameter ("pinhole size"). Of the above parameters, only exciting light and pinhole size varied among experiments. The program used their recorded values, together with empirical functions, to correct the fluorescence intensity to a standard scanner setting.

The Calculation of Event Frequency

Event frequency f was calculated in every image by dividing number of events by extent of the image within the fiber (in 100-μm units) and elapsed time (which was 0.64 s in line scans and three times greater in x-y images, due to triple interleaving). f was calculated by the same formula in line scans or x-y images. In both types of images, time progresses linearly along the y axis; in both, f is equal to number of events divided by scanned length (i.e., the extent of the x axis inside the fiber) and by the time elapsed while the image is obtained. Because there is no a priori information on location of sources, the probability of sparks must be assumed to be the same in any volume element within the cell; hence, it should not matter for the resulting frequency whether scanning is in x and y (i.e., new volumes are scanned), or is repeated along the same line at constant y (and the same volume elements are sampled repeatedly). One trivial adjustment was made for the calculation of f in x-y scans: if fiber width varied with y, then the average width was used as divisor.

Data Groups and Statistics

$F_3(x, t)$ images suitable for evaluation of sparks were acquired in groups of 50 (named "series"), which were bracketed by measurements of $[Ca^{2+}]_{SR}$. Hence each series has a defined $[Ca^{2+}]_{SR}$ (the average of its bracketing values), an event frequency and an average value of each morphometric parameter. At least three series were recorded in each of 16 experiments with changes in $[Ca^{2+}]_{SR}$. 60 series were left after discarding those obtained at times earlier than 10 min after permeabilization and those where f was too low for reliable parameter estimation (less than 1 $[100\ \mu m]^{-1}s^{-1}$). They include a total of 16,415 events. To a large extent, the evaluation of properties of sparks was based on these series-averaged parameters. Other analyses were based on averages by individual cell, or averages and correlations over all events.

Significance of paired differences was assessed by Student's two-tailed t test. Significance of correlations was established by tests on the sample coefficient of determination r^2 based on the distribution of Pearson's correlation coefficient r or its logarithmic transform z (e.g., Cramér, 1946).

RESULTS

Several studies (e.g., Klein et al., 1996; Zhou et al., 2004) have shown that frequency and other properties of sparks depend steeply on cytosolic $[Ca^{2+}]$. Hence, to define the effect of $[Ca^{2+}]_{SR}$ it was necessary to maintain a constant $[Ca^{2+}]_{cyto}$ during collection of sparks. Changes of $[Ca^{2+}]_{SR}$ were induced using procedures defined earlier (Launikonis et al., 2005). To increase $[Ca^{2+}]_{SR}$, $[Ca^{2+}]_{cyto}$ was transiently elevated (to 400 or 800 nM) and then returned to 100 nM, the concentration at which sparks were collected. Conversely, to lower $[Ca^{2+}]_{SR}$, we used exposure to the relaxing solution, with $[Ca^{2+}] < 10^{-8}$ M, which causes rapid leak through the SR Ca^{2+} pump (Launikonis and Stephenson, 1997; Macdonald and Stephenson, 2001; Launikonis et al., 2005).

$[Ca^{2+}]_{SR}$ Could Be Changed Reversibly

Sixteen cells were subjected to changes in $[Ca^{2+}]_{SR}$. A representative experiment is illustrated in Fig. 2. The single fiber, dissected from a muscle preloaded in

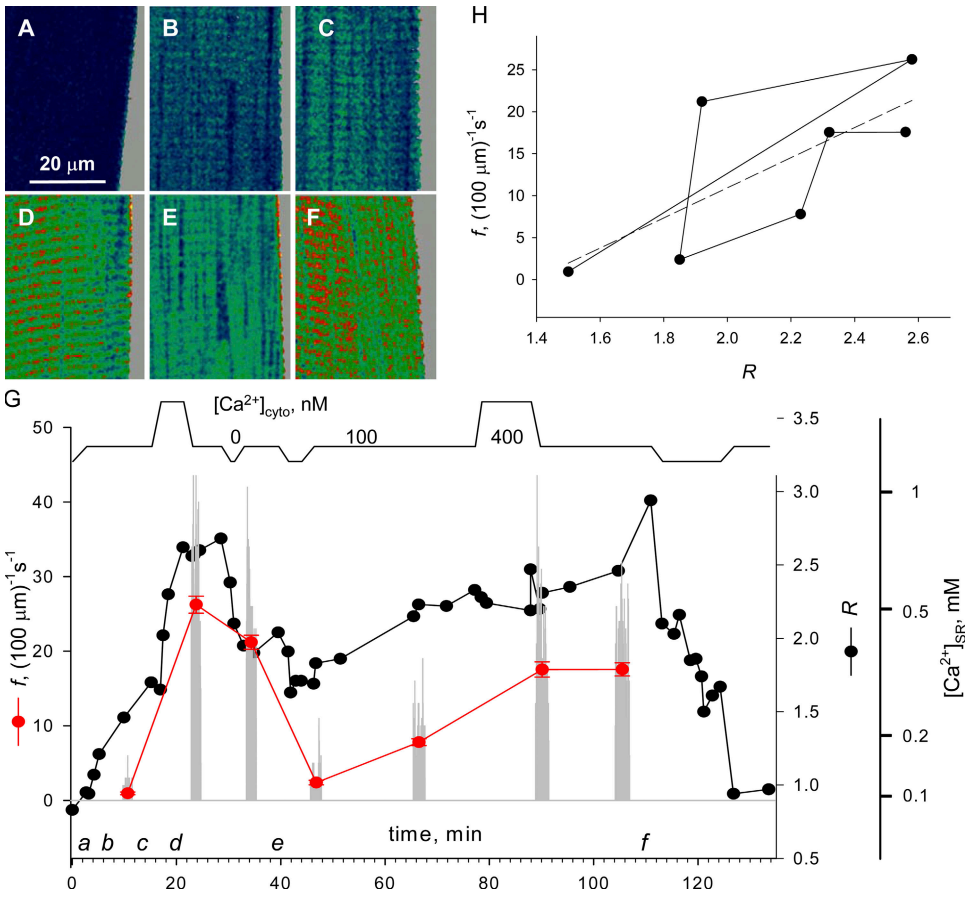

Figure 2. Interventions that change $[Ca^{2+}]_{SR}$. (A–F) Representative SEER ratio images of fluorescence of mag-indo-1 trapped inside organelles of a membrane-permeabilized muscle fiber. (G, top) Schematic representation of $[Ca^{2+}]$ in perfusing solutions, including the reference (100 nM), a high Ca^{2+} saline (400 nM) and relaxing solution (~10 nM). Black symbols and lines plot *R*, SEER ratio averaged over well-stained regions of the image. Gray bars, the frequency of sparks detected in individual line scan images. Red symbols, *f*, average spark frequency (±SEM) within series of 50 line scan images. Right offset axis, $[Ca^{2+}]$ corresponding to *R*. Identifier: 061004a.

mag-indo-1 AM, was mounted for imaging and permeabilized in relaxing solution containing rhod-2. The cytosolic solution was then changed while images of SEER ratio (monitoring $[Ca^{2+}]_{SR}$) and rhod-2 fluorescence (for $[Ca^{2+}]_{cyto}$) were acquired. Representative ratio images are in Fig. 2 (A–F). In the timeline in panel G, the applied $[Ca^{2+}]$ in the cytosolic solutions is plotted schematically at top and times of images A–F are indicated as *a–f*. Sojourns in either high or very low $[Ca^{2+}]_{cyto}$ (<10 nM, in solutions without ATP) were bracketed with intervals in physiological $[Ca^{2+}]_{cyto}$ (100 nM), during which one to three series of 50 line scan images of fluorescence of rhod-2 were collected. The gray vertical bars in Fig. 2 G represent as diary plot the event frequency *f* measured in every image. The black symbols represent the cell-averaged SEER ratio, *R*. In this and other graphs we preserve the "raw" measurement *R*, and on an additional axis present corresponding values of $[Ca^{2+}]_{SR}$, derived using Eq. 1 and parameter values of Launikonis et al. (2005). Within the range of values attained in the present experiments, $[Ca^{2+}]_{SR}$ is approximately proportional to $R - 0.4$.

Several features of the evolution of *R* that are evident in the example are representative of most cells treated this way. The initial value upon membrane permeabilization (derived from Fig. 2 A), corresponded to a $[Ca^{2+}]_{SR}$ between 50 and 100 μM ; $[Ca^{2+}]_{SR}$ increased sharply upon exposure to 100 nM $[Ca^{2+}]_{cyto}$ (Fig. 2, B and C); the increase was enhanced by exposure to higher $[Ca^{2+}]_{cyto}$ (D), and was largely irreversible upon returning to reference solution. To reduce $[Ca^{2+}]_{SR}$, the cell had to be placed in a nominally Ca^{2+}-free solution (Fig. 2 E was obtained afterwards). Sparks could thus be collected in 100 nM $[Ca^{2+}]_{cyto}$, at $[Ca^{2+}]_{SR}$ values ranging from <100 nM to ~1.2 mM.

Spark Frequency Increased after Membrane Permeabilization

The experiment of Fig. 2 is illustrative of the evolution of *f*, which in most, but not all, cells increased after exposure to high $[Ca^{2+}]_{cyto}$ and then decreased under conditions that diminished $[Ca^{2+}]_{SR}$. Fig. 2 H indicates a rough correlation. But to establish the association between frequency and $[Ca^{2+}]_{SR}$ required taking into consideration another variable, which Isaeva and Shirokova (2003) first reported to affect *f*, namely the time elapsed after membrane permeabilization.

The importance of elapsed time is illustrated in Fig. 3, which summarizes data from 19 experiments as 3-D plots of *f* vs. time elapsed after membrane permeabilization, and vs. measured *R*. $[Ca^{2+}]_{cyto}$ was 100 nM in every case. Values of *f* and *R* were calculated in triple interleaved *x-y* scans as described in Materials and Methods.

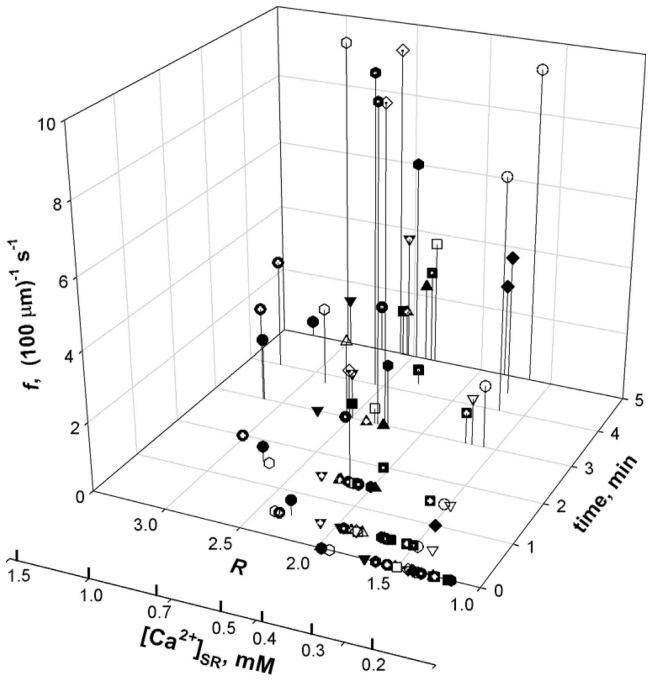

Figure 3. Early evolution of spark frequency. *f*, computed in *x-y* scans, as a function of time after membrane permeabilization and average of *R* in simultaneous line-interleaved *x-y* images. Different symbols correspond to different experiments (19 fibers).

TABLE I

Spontaneous Evolution of Sparks Frequency and $[Ca^{2+}]_{SR}$ in Reference Solution

Fiber	*f*	*f*	Δ *f*	*R*	*R*	Δ *R*
	10 min	20 min		10 min	20 min	
051904b	0.40	1.30	0.90	2.00	2.15	0.15
061704a	1.70	2.40	0.70	1.90	2.30	0.40
062104b	1.90	1.70	−0.20	1.65	1.65	0.00
062104c	1.80	3.70	1.90	1.50	1.65	0.15
070204b	1.60	1.70	0.10	1.70	1.60	−0.10
070704b	9.00	12.00	3.00	1.60	1.40	−0.20
070904a	10.10	10.30	0.20	1.67	1.67	0.00
average	3.79	4.73	0.94[a]	1.72	1.77	0.06
SEM	1.51	1.69	0.43	0.07	0.12	0.07

f, spark frequency in series of 50 images collected 10 or 20 minutes after membrane permeabilization, in fibers that remained in reference solution throughout. Column 4 lists differences between columns 3 and 2. *R*, average SEER ratio in measures bracketing the sets of line scans used for calculating *f*. Column 7 lists the differences between columns 6 and 5. Row labeled "SEM" lists standard errors of the means above.
[a]Significant difference.

Regardless of the measured *R*, events were not detected for 2 or 3 min after permeabilization, and then their frequency increased, tending to stabilize by 6–10 min. Because all fibers start with low $[Ca^{2+}]_{SR}$ after saponin treatment, the rapid increase in *f* could be due in part to the increase in $[Ca^{2+}]_{SR}$ that occurs in virtually every fiber. However, no sparks were observed even in the occasional fibers that started with elevated $[Ca^{2+}]_{SR}$; therefore, an additional mechanism must be at work. A similar phenomenon occurs in mammalian muscle, in which the increase is attributed to an excess of reactive oxygen species (Isaeva and Shirokova, 2003; Isaeva et al., 2005).

Looking for an end point in this spontaneous evolution of spark frequency, we recorded in seven fibers events and $[Ca^{2+}]_{SR}$, without modifying conditions for >20 min. The results are summarized in Table I, which lists *f* and *R* at 10 and 20 min. Between 10 and 20 min, *R* changed by 0.06 ($P > 0.1$, $n = 7$) corresponding to a change in $[Ca^{2+}]_{SR}$ of ∼5%. *f* increased by ∼20% in the same interval ($P < 0.05$). Spark "morphologic" parameters (amplitude, FWHM, and rise time) did not change significantly. In conclusion, spark frequency increased dramatically during the first few minutes after membrane permeabilization. This increase, which may be unrelated to the concomitant growth in $[Ca^{2+}]_{SR}$, tended to stabilize with time. Between 10 and 20 min it amounted to ∼10% of the value of *f* at 10 min, as justified below. This spontaneous baseline change must be taken into account before ascribing further changes to additional factors.

Given this result, our standard procedure was to wait for 10 min in reference solution after permeabilization, acquire a reference set of line scans for evaluation of sparks, and then proceed to solution changes designed to increase and later decrease $[Ca^{2+}]_{SR}$. The measured *R* changed substantially upon the interventions, encompassing values corresponding to 0.05 to 1.2 mM $[Ca^{2+}]$. In complete experiments, $[Ca^{2+}]_{SR}$ measured at ∼10 min after permeabilization averaged 0.268 (±0.015) mM, and increased to 0.442 (±0.052) mM after the passage through high $[Ca^{2+}]_{cyto}$. After the time in reference solution (i.e., 100 nM $[Ca^{2+}]$) needed for acquisition of spark images at elevated SR load, $[Ca^{2+}]_{SR}$ had decreased to 0.426 (0.045) mM; then after exposure to relaxing solution, $[Ca^{2+}]_{SR}$ decreased to 0.323 (0.023) mM. Both the increase during the passage through high $[Ca^{2+}]_{cyto}$ and the decrease in relaxing solution were statistically highly significant ($P < 0.01$, $n = 10$). In summary, we were able to increase the value of the controlling variable $[Ca^{2+}]_{SR}$ by ∼65% and then return it to near its initial value. This return is crucial to approximately offset the effect of time and the associated slow increase in *f*. Therefore, experiments in which the fiber showed indications of decay upon exposure to relaxing solution were discarded. Of 16 experiments with changes in $[Ca^{2+}]_{SR}$, 10 were used to compute average effects on $[Ca^{2+}]_{SR}$ and event frequency.

Spark Frequency Was Modified by Changes in $[Ca^{2+}]_{SR}$

f changed with $[Ca^{2+}]_{SR}$. The red symbols in Fig. 2 G represent averages of *f* in each series. In Fig. 2 H, *f* plotted vs. *R* reveals a positive correlation, which was

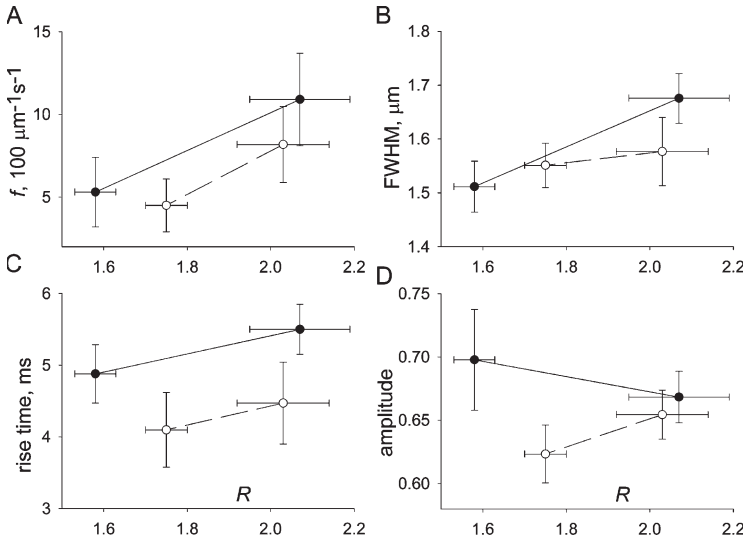

Figure 4. Spark parameters at different $[Ca^{2+}]_{SR}$. (A) Averages over all fibers of *R* vs. *f* in four conditions: filled symbols, before or after exposure to high $[Ca^{2+}]_{cyto}$; open symbols, before or after exposure to relaxing solution. (B–D) Averages of morphologic spark parameters, first computed for individual fibers ($n = 10$), and then averaged over fibers and plotted as described for A. Bars represent the standard error of the mean over fibers.

observed in most experiments. The collective changes in frequency are represented in two ways. In Fig. 4 A, *f* averaged in all experiments is plotted vs. average *R* before and after the exposure to high $[Ca^{2+}]_{cyto}$ (filled symbols), or before and after exposure to relaxing solution. The plot shows a reversible increase, but the changes are not statistically significant. A different analysis is presented in Table II, where columns 2 and 3 list averages (and SEMs) of frequency and morphologic spark parameters, respectively, at "low" and "high" $[Ca^{2+}]_{SR}$. Averages at low $[Ca^{2+}]_{SR}$ pool values in series acquired before the $[Ca^{2+}]$-increasing exposure and in series after the $[Ca^{2+}]$-decreasing intervention. Averages at high $[Ca^{2+}]_{SR}$ pool values after the $[Ca^{2+}]$ increase and those before the $[Ca^{2+}]$ decrease. These averages therefore summarize the effect of changing $[Ca^{2+}]_{SR}$ and offset the time-associated drift. Column 4 in Table II lists the averaged fiber-paired differences and their SEMs. The changes in *R* and *f* associated with the interventions were significant in two-tailed *t* tests ($P < 0.05$).

The average results in Table II yield a rough measure of the magnitude of the effect (others are given in Discussion). A 45% increase in $[Ca^{2+}]_{SR}$ from 299 to 433 μM was accompanied by a 93% increase in *f*. By linear interpolation, the 5% increase in $[Ca^{2+}]_{SR}$ that occurred between 10 and 20 min in cells left in reference solution would increase *f* by ~10%. Hence our estimate that the spontaneous increase in *f* during this time that is not attributable to the change in $[Ca^{2+}]_{SR}$ was of the order of 10%.

Part of the reason that changes in *R* were limited and those in *f* were only moderately significant was the inclusion of two cells (of 16) in which exposure to a high $[Ca^{2+}]_{cyto}$ led to a sudden decrease in $[Ca^{2+}]_{SR}$ and three others in which the increase in $[Ca^{2+}]_{SR}$ was associated with a reduction or no change in *f*. The observations were in line with a previous report that high $[Ca^{2+}]_{cyto}$ applied early in an experiment increased *f*, but caused the opposite effect after passages through solutions of intermediate $[Ca^{2+}]$ (Zhou et al., 2004). Possible implications of this hysteretic effect will be discussed later.

At the other end of the range, in one experiment the exposure to high $[Ca^{2+}]_{cyto}$ resulted in a threefold increase in $[Ca^{2+}]_{SR}$ (to 0.8 mM) with a 3.5-fold increase in *f* (to 25 $[100\ \mu m]^{-1}s^{-1}$). Even though *f* values up to 35 $(100\ \mu m)^{-1}s^{-1}$ were observed and many sparks were clearly propagating in space, there was never a progression to uncontrolled Ca^{2+} release or cell-wide waves.

Spark Morphology Was Modified Slightly by Changes in $[Ca^{2+}]_{SR}$

The approach to examine changes in spark morphologic parameters was similar to the analysis of changes

TABLE II

Sparks Frequency and Morphology at Different $[Ca^{2+}]_{SR}$

	Low Ca	High Ca	Δ	*n*
R	1.6781	2.0476	0.370[a]	10
SEM	0.0392	0.0812	0.087	
f	4.8333	9.3429	4.510[a]	10
SEM	1.2816	1.7734	1.696	
FWHM	1.5338	1.6200	0.086	7
SEM	0.0305	0.0417	0.039	
Rise time	4.4653	4.9554	0.490	7
SEM	0.3572	0.2720	0.272	
Amplitude	0.6584	0.6610	0.003	7
SEM	0.0234	0.0137	0.022	

A "low Ca" and a "high Ca" value of the parameters listed were calculated for each fiber as described in the text. Column 4 (Δ) lists averages of fiber-paired differences, and their standard errors. *n* is number of experiments. Three fibers where *f* was very low (<1.0) were not included in the calculation of morphologic parameter averages.

[a]Significant difference.

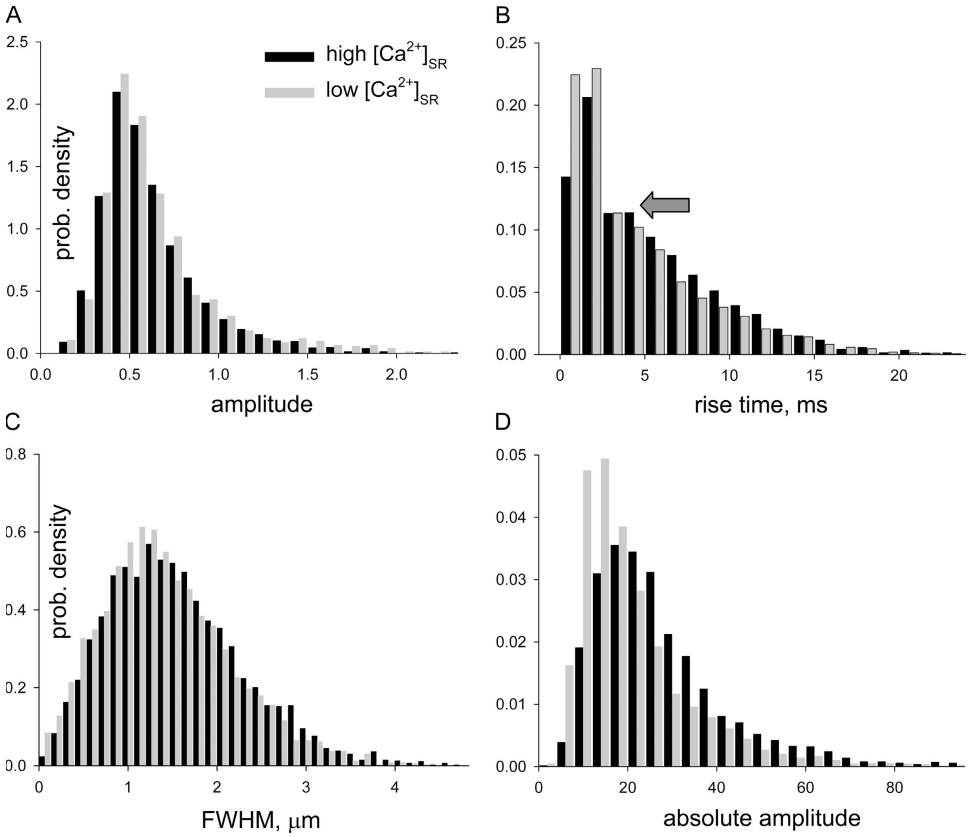

Figure 5. Effects of $[Ca^{2+}]_{SR}$ on morphologic spark parameters. Histograms of parameter values of individual sparks in all fibers included in Table II. Black bars represent the high $[Ca^{2+}]_{SR}$ condition and gray bars the low $[Ca^{2+}]_{SR}$ condition. (A) Histogram of conventionally defined amplitudes. (B) Histogram of rise times. The arrow marks a minor mode, visible in this histogram in both conditions. (C) Histogram of FWHM. (D) Histogram of absolute amplitudes, calculated as described in Materials and Methods. Note that the histogram of absolute amplitudes changes with $[Ca^{2+}]_{SR}$, whereas that of conventionally defined amplitudes does not.

in *f*. In Fig. 4 (B–D), mean values are plotted vs. average *R*. *R* values are the same in all graphs. While spatial width (Fig. 4 B) and rise time (C) correlated positively with *R*, spark amplitude did not. The paired statistical analysis in Table II establishes that the increase in $[Ca^{2+}]_{SR}$ was accompanied by small and barely significant increases in spatial width (6%) and rise time (11%, $P < 0.1$) and a negligible change in amplitude.

A complementary view of the effect of $[Ca^{2+}]_{SR}$ on spark morphology is presented in Fig. 5, comparing the histograms of amplitude (Fig. 5 A), rise time (B), and spatial width (C) in all sparks in high $[Ca^{2+}]_{SR}$ (black bars) with those in low Ca^{2+} (gray). In both conditions, the distribution of amplitudes was basically a monotonic decay (except at the lowest amplitudes where probability density increases with amplitude, due to missed events). This well known tendency, which reflects the sharp off-focus decay of measured fluorescence intensity (Cheng et al., 1999; Ríos et al., 2001), was of course indifferent to changes in $[Ca^{2+}]_{SR}$. The histogram of rise times was monotonically decaying as well, but for the hint of a mode near 4 ms (arrow). This mode was described before (Ríos et al., 2001) and assigned to nonequilibrium interactions among channels, mediated by the increase in $[Ca^{2+}]$ near the cytosolic face of open RyRs. The effects of changes in $[Ca^{2+}]_{SR}$ on either rise time or spatial width histograms were minor, consistent with the small value of the paired differences listed in Table II.

An increased spark rise time at high $[Ca^{2+}]_{SR}$ reveals a slight increase in underlying release current duration. This change and the greater driving force should have resulted in increased spark amplitude. Seeking to explain the absence of the expected increase we noticed that the resting fluorescence F_0, which enters the calculation of spark amplitude as a normalization factor, often increased at high $[Ca^{2+}]_{SR}$, a change that could be nearly twofold when the increases in *f* were major. The association with *f* suggests that the increase in F_0 may have resulted from imperfect elimination of "sparky" areas in images of high *f*; it could also be the consequence of steady activation of channels, which resulted in actual increase in resting $[Ca^{2+}]_{cyto}$, or it could reflect contributions from undetected, out of focus sparks. In an alternative study, the peak change in fluorescence was determined on original images, without normalization. The determination of this "absolute amplitude" is described in detail in Materials and Methods. Given that the total dye concentration was always the same, absolute amplitude should be simply related to the local increase in $[Ca^{2+}]_{cyto}$. Fig. 5 D plots its histograms in high and low $[Ca^{2+}]_{SR}$ and shows that, as expected, in high $[Ca^{2+}]_{SR}$, absolute amplitudes were generally higher. Averages were 20.1 (± 0.12, $n = 3057$ events) in low $[Ca^{2+}]_{SR}$ and 27.7 (± 0.19, $n = 5530$) in high $[Ca^{2+}]_{SR}$, a 38% change. The increases in absolute amplitude paired by fiber were highly significant ($P < 0.05$, $n = 7$).

DISCUSSION

The present study characterizes for the first time properties of Ca^{2+} sparks under variable, directly measured concentrations of free Ca^{2+} in the SR. The main outcome is that increased skeletal muscle $[Ca^{2+}]_{SR}$ promotes Ca^{2+} sparks, but the magnitude of this effect is less than in heart muscle. The frequency of sparks increased more than proportionally with the change in $[Ca^{2+}]_{SR}$; the rise time and spatial width increased only slightly and amplitude increased significantly, provided that the comparison was made without normalizing by resting fluorescence. Technical constraints limited the achievable range of changes in $[Ca^{2+}]_{SR}$ to a less than twofold increase from the steady level reached in 100 nM $[Ca^{2+}]_{cyto}$. It is possible that disproportionately greater levels of activation will be reached upon greater increases in SR load, as has been shown for cardiac muscle (Shannon et al., 2000). Such nonlinear activation was not found, however, in any individual experiment, including those that reached the highest values of $[Ca^{2+}]_{SR}$.

$[Ca^{2+}]_{SR}$ Is a Minor Determinant of Spark Frequency

The effects of increased $[Ca^{2+}]_{SR}$ were measurable, but small in terms of the dispersion of parameter values. Specifically, the differences in averages illustrated in Fig. 4 were not significant for any of the variables. Only the paired differences, listed in Table II, were statistically significant, which implies that the variability among fibers was enough to obscure the effect of $[Ca^{2+}]_{SR}$. Two quantitative indications of the importance of $[Ca^{2+}]_{SR}$ in determining f are presented with Fig. 6. In Fig. 6 A series-averaged R was plotted vs. series-averaged f (see Materials and Methods). Fig. 6 B is the joint histogram of f and R for the whole sample of 16415 sparks, with two-dimensional bin frequency represented in color. First order regression lines are plotted in both cases. The regression of the scatter plot (Fig. 6 A) gives equal weight to each series, whereas the regression of the histogram (Fig. 6 B) weights all events equally. In Fig. 6 A, the correlation coefficient r is 0.1, which is not different from zero for this sample of 60 value pairs. For the joint histogram, r is 0.24, which is significantly different from zero. The second choice of variables allows a simple decomposition of the variance. The variance of f explained by the dependence on R (i.e., $[(f_p - f_m)]^2$, where f_p is the predicted value of frequency according to its linear dependence on R and f_m the sample average) was just 5.7% of the total sample variance $[(f - f_m)]^2$. An equivalent measure of strength of the correlation is given by the coefficient of determination $r^2 = 0.0576$ (e.g., Hill and Lewicki, 2006).

The present observation of weak effects of $[Ca^{2+}]_{SR}$ on spark properties should be considered together with the finding that only a small local depletion occurs during a spark (Launikonis et al., 2006) and that limited depletion occurs after release elicited by an action potential (Pape et al., 1993). Taken together with these studies, the present results contradict the consensus, emergent in cardiac muscle, that depletion of Ca^{2+} mediates termination of sparks. Similarly, the results do not support a role for SR depletion in the fast spontaneous decay of Ca^{2+} release observed at the cell-wide level in frog skeletal muscle (Baylor et al., 1983; Melzer et al., 1984; Schneider and Simon, 1988), a decay believed to reflect the termination of Ca^{2+} release in sparks (Shirokova et al., 1996).

Previous studies of Ca^{2+} release at the whole-cell level found an increase in release permeability induced by membrane voltage as SR load decreased (Pape and Carrier, 1998; Pape et al., 1998; Posterino and Lamb, 2003; Pizarro and Ríos, 2004), which appears to conflict with the present observation of greater event frequency at higher load. This divergence in the effects of load is

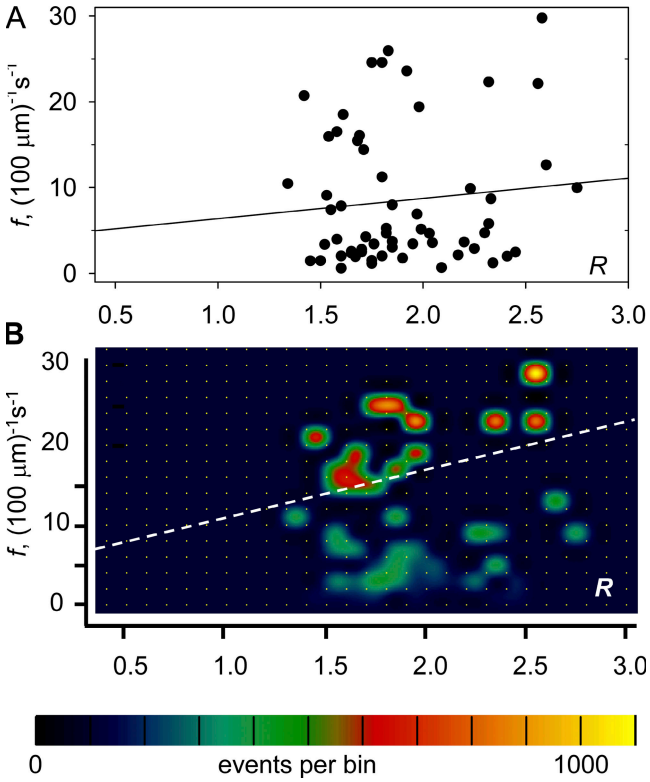

Figure 6. The correlation of $[Ca^{2+}]_{SR}$ and event frequency. (A) Each data point represents a series of 50 images by the average of two measurements of R, which bracket the series, vs. the series-averaged event frequency f. The first order regression line has slope 2.35 $(100\ \mu m)^{-1}s^{-1}$ and intercept 4.04 $(100\ \mu m)^{-1}s^{-1}$. r is 0.10. (B) The joint histogram of R and f in individual events. Every event in a series is given the same values of R and f. The histogram is different from zero only in bins containing the pairs of values plotted in A. Bin frequency is encoded in color and interpolated for visibility as described by González et al., (2000). The regression line has slope 5.28 $(100\ \mu m)^{-1}s^{-1}$ and intercept 5.35 $(100\ \mu m)^{-1}s^{-1}$. r is 0.24. By weighing every event equally, the regression in B uncovers a positive correlation between the variables.

consistent with the conclusion of Lamb et al. (2001) that two forms of Ca^{2+} release, that induced by caffeine (a proxy for CICR and its local manifestation in sparks) and that induced by membrane depolarization, have opposite sensitivities to SR load. Taken together, local and global measurements indicate that the enhancement of channel opening by increase in load constitutes a minor factor in the physiological voltage-controlled Ca^{2+} release in skeletal muscle.

Control by Lumenal Calcium in Skeletal and Cardiac Muscle

Our largely negative conclusions are in contrast with the consensus in cardiac muscle, in which SR load appears to critically determine spark duration (Terentyev et al., 2002), frequency (Györke et al., 1997), diastolic leak (Shannon et al., 2000), and even refractoriness and arrhythmias (Terentyev et al., 2003). The most striking manifestation of the functional differences between the two muscle types is the dissimilar local depletion associated with sparks: "blinks" that reduce $[Ca^{2+}]_{SR}$ by 54% in cardiac muscle versus "skraps" of $<7\%$ in skeletal muscle. Structural features of cardiac muscle, including terminal cisternae of much smaller volume (Brochet et al., 2005; Mobley and Eisenberg, 1975), containing less quantity (Volpe et al., 1988) of a calsequestrin isoform that has a lower binding capacity (Park et al., 2004), probably explain the functional differences with skeletal muscle.

The mild effects of $[Ca^{2+}]_{SR}$ on frequency and spark morphology result from averaging a majority of cells where the effects were substantial, as in Fig. 2, together with a few cells in which the changes were nil or negative. The "rogue" effects were reminiscent of an earlier observation of hysteresis in the response to $[Ca^{2+}]_{cyto}$. The observation, which was made without measuring $[Ca^{2+}]_{SR}$, was that high $[Ca^{2+}]_{cyto}$ applied early in an experiment increased spark frequency, but the same solution caused the opposite effect if applied later, after passages through solutions of intermediate $[Ca^{2+}]$ (Zhou et al., 2004). Taken together, hysteresis and variability of the response emphasize that important determinants of channel properties and Ca^{2+} release in skeletal muscle remain uncontrolled and unknown. Launikonis et al. (2006) have suggested one likely determinant, the aggregation state of the intra-SR buffer calsequestrin, which has been shown to be sensitive to $[Ca^{2+}]$ and to determine the Ca^{2+} binding properties of the protein in aqueous suspensions (Park et al., 2004).

We are grateful to Tom DeCoursey for many helpful suggestions.

This work was supported by grants from National Institute of Arthritis and Musculoskeletal and Skin Diseases/National Institutes of Health to E. Ríos. B.S. Launikonis was a C.J. Martin Fellow of the National Health and Medical Research Council (Australia).

Olaf S. Andersen served as editor.

Submitted: 23 March 2006
Accepted: 26 May 2006

REFERENCES

Baylor, S.M., W.K. Chandler, and M.W. Marshall. 1983. Sarcoplasmic reticulum calcium release in frog skeletal muscle fibres estimated from Arsenazo III calcium transients. *J. Physiol.* 344:625–666.

Beard, N.A., M.G. Casarotto, L. Wei, M. Varsanyi, D.R. Laver, and A.F. Dulhunty. 2005. Regulation of ryanodine receptors by calsequestrin: effect of high luminal Ca^{2+} and phosphorylation. *Biophys. J.* 88:3444–3454.

Brochet, D.X., D. Yang, A. Di Maio, W.J. Lederer, C. Franzini-Armstrong, and H. Cheng. 2005. Ca^{2+} blinks: rapid nanoscopic store calcium signaling. *Proc. Natl. Acad. Sci. USA.* 102:3099–3104.

Cheng, H., L.S. Song, N. Shirokova, A. González, E.G. Lakatta, E. Ríos, and M.D. Stern. 1999. Amplitude distribution of calcium sparks in confocal images: theory and studies with an automatic detection method. *Biophys. J.* 76:606–617.

Cramér, H. 1946. Mathematical Methods of Statistics. Princeton University Press, Princeton, NJ. 467.

Endo, M., M. Tanaka, and Y. Ogawa. 1970. Calcium induced calcium release of calcium from the sarcoplasmic reticulum of skinned skeletal muscle fibres. *Nature.* 228:34–36.

González, A., W.G. Kirsch, N. Shirokova, G. Pizarro, G. Brum, I.N. Pessah, M.D. Stern, H. Cheng, and E. Ríos. 2000. Involvement of multiple intracellular release channels in calcium sparks of skeletal muscle. *Proc. Natl. Acad. Sci. USA.* 97:4380–4385.

Györke, I., N. Hester, L.R. Jones, and S. Györke. 2004. The role of calsequestrin, triadin, and junctin in conferring cardiac ryanodine receptor responsiveness to luminal calcium. *Biophys. J.* 86:2121–2128.

Györke, S., V. Lukyanenko, and I. Györke. 1997. Dual effects of tetracaine on spontaneous calcium release in rat ventricular myocytes. *J. Physiol.* 500:297–309.

Györke, S., I. Györke, V. Lukyanenko, D. Terentyev, S. Viatchenko-Karpinski, and T.F. Wiesner. 2002. Regulation of sarcoplasmic reticulum calcium release by luminal calcium in cardiac muscle. *Front. Biosci.* 7:d1454–d1463.

Hill, T., and P. Lewicki. 2006. Statistics Methods and Applications. StatSoft, Tulsa, OK. http://www.statsoft.com/textbook/stathome.html.

Isaeva, E.V., and N. Shirokova. 2003. Metabolic regulation of Ca^{2+} release in permeabilized mammalian skeletal muscle fibres. *J. Physiol.* 547:453–462.

Isaeva, E.V., V.M. Shkryl, and N. Shirokova. 2005. Mitochondrial redox state and Ca^{2+} sparks in permeabilized mammalian skeletal muscle. *J. Physiol.* 565:855–872.

Klein, M.G., H. Cheng, L.F. Santana, Y.H. Jiang, W.J. Lederer, and M.F. Schneider. 1996. Two mechanisms of quantized calcium release in skeletal muscle. *Nature.* 379:455–458.

Lamb, G.D., M.A. Cellini, and D.G. Stephenson. 2001. Different Ca^{2+} releasing actions of caffeine and depolarization in skeletal muscle fibres from rat. *J. Physiol.* 531:715–728.

Launikonis, B.S., and D.G. Stephenson. 1997. Effect of saponin treatment on the sarcoplasmic reticulum of rat, cane toad and crustacean (yabby) skeletal muscle. *J. Physiol.* 504:425–437.

Launikonis, B.S., J. Zhou, L. Royer, T.R. Shannon, G. Brum, and E. Ríos. 2005. Confocal imaging of $[Ca^{2+}]$ in cellular organelles by SEER, shifted excitation and emission ratioing. *J. Physiol.* 567:523–543.

Launikonis, B.S., J. Zhou, L. Royer, T.R. Shannon, G. Brum, and E. Ríos. 2006. Depletion "skraps" and dynamic buffering inside the cellular Ca^{2+} store. *Proc. Natl. Acad. Sci. USA.* 103:2982–2987.

Macdonald, W.A., and D.G. Stephenson. 2001. Effects of ADP on sarcoplasmic reticulum function in mechanically skinned skeletal muscle fibres of the rat. *J. Physiol.* 532:499–508.

Melzer, W., E. Ríos, and M.F. Schneider. 1984. Time course of calcium release and removal in skeletal muscle fibers. *Biophys. J.* 45:637–641.

Mobley, B.A., and B.R. Eisenberg. 1975. Sizes of components in frog skeletal muscle measured by methods of stereology. *J. Gen. Physiol.* 66:31–45.

Pape, P.C., and N. Carrier. 1998. Effect of sarcoplasmic reticulum (SR) calcium content on SR calcium release elicited by small voltage-clamp depolarizations in frog cut skeletal muscle fibers equilibrated with 20 mM EGTA. *J. Gen. Physiol.* 112:161–179.

Pape, P.C., D.S. Jong, W.K. Chandler, and S.M. Baylor. 1993. Effect of fura-2 on action potential-stimulated calcium release in cut twitch fibers from frog muscle. *J. Gen. Physiol.* 102:295–332.

Pape, P.C., D.S. Jong, and W.K. Chandler. 1998. Effects of partial sarcoplasmic reticulum calcium depletion on calcium release in frog cut muscle fibers equilibrated with 20 mM EGTA. *J. Gen. Physiol.* 112:263–295.

Park, H., I.Y. Park, E. Kim, B. Youn, K. Fields, A.K. Dunker, and C. Kang. 2004. Comparing skeletal and cardiac calsequestrin structures and their calcium binding: a proposed mechanism for coupled calcium binding and protein polymerization. *J. Biol. Chem.* 279:18026–18033.

Pizarro, G., and E. Ríos. 2004. How source content determines intracellular Ca^{2+} release kinetics. Simultaneous measurement of [Ca^{2+}] transients and [H^{+}] displacement in skeletal muscle. *J. Gen. Physiol.* 124:239–258.

Posterino, G.S., and G.D. Lamb. 2003. Effect of sarcoplasmic reticulum Ca^{2+} content on action potential-induced Ca^{2+} release in rat skeletal muscle fibres. *J. Physiol.* 551:219–237.

Ríos, E., N. Shirokova, W.G. Kirsch, G. Pizarro, M.D. Stern, H. Cheng, and A. González. 2001. A preferred amplitude of calcium sparks in skeletal muscle. *Biophys. J.* 80:169–183.

Rome, L.C. 2006. Design and function of superfast muscles: new insights into physiology of skeletal muscle. *Annu. Rev. Physiol.* 68:193–221.

Schneider, M.F., and B.J. Simon. 1988. Inactivation of calcium release from the sarcoplasmic reticulum in frog skeletal muscle. *J. Physiol.* 405:727–745.

Shannon, T.R., K.S. Ginsberg, and D.M. Bers. 2000. Potentiation of fractional sarcoplasmic reticulum calcium release by total and free intra-sarcoplasmic reticulum calcium concentration. *Biophys. J.* 78:334–343.

Shirokova, N., J. García, G. Pizarro, and E. Ríos. 1996. Ca^{2+} release from the sarcoplasmic reticulum compared in amphibian and mammalian skeletal muscle. *J. Gen. Physiol.* 107:1–18.

Terentyev, D., S. Viatchenko-Karpinski, H.H. Valdivia, A.L. Escobar, and S. Györke. 2002. Luminal Ca^{2+} controls termination and refractory behavior of Ca^{2+}-induced Ca^{2+} release in cardiac myocytes. *Circ. Res.* 91:414–420.

Terentyev, D., S. Viatchenko-Karpinski, I. Györke, P. Volpe, S.C. Williams, and S. Györke. 2003. Calsequestrin determines the functional size and stability of cardiac intracellular calcium stores: mechanism for hereditary arrhythmia. *Proc. Natl. Acad. Sci. USA.* 100:11759–11764.

Tripathy, A., and G. Meissner. 1996. Sarcoplasmic reticulum lumenal Ca^{2+} has access to cytosolic activation and inactivation sites of skeletal muscle Ca^{2+} release channel. *Biophys. J.* 70:2600–2615.

Volpe, P., M. Bravin, F. Zorzato, and A. Margreth. 1988. Isolation of terminal cisternae of frog skeletal muscle. Calcium storage and release properties. *J. Biol. Chem.* 263:9901–9907.

Zhou, J., B.S. Launikonis, E. Ríos, and G. Brum. 2004. Regulation of Ca^{2+} sparks by Ca^{2+} and Mg^{2+} in mammalian and amphibian muscle. An RyR isoform-specific role in excitation–contraction coupling? *J. Gen. Physiol.* 124:409–428.